Virology 599 (2024) 110198

Contents lists available at ScienceDirect

Virology

journal homepage: www.elsevier.com/locate/virology

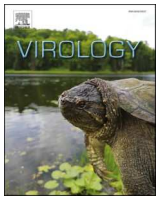

Conserved sequence features in intracellular domains of viral spike proteins

Vinh-Nhan Ngo [a,1], David P. Winski [a], Brandon Aho [a], Pauline L. Kamath [b], Benjamin L. King [c], Hang Waters [d], Joshua Zimmerberg [d], Alexander Sodt [e], Samuel T. Hess [a,*,1]

[a] Department of Physics and Astronomy, 120 Bennett Hall, University of Maine, Orono, ME, 04469-5709, USA
[b] School of Food and Agriculture, 342 Hitchner Hall, University of Maine, And Maine Center for Genetics in the Environment, Orono, ME, USA
[c] Department of Molecular and Biomedical Sciences, 5735 Hitchner Hall, University of Maine, Orono, ME, USA
[d] Section on Integrative Biophysics, Eunice Kennedy Shriver National Institute of Child Health and Human Development, National Institutes of Health, Bethesda, MD, USA
[e] Unit on Membrane Chemical Physics, Eunice Kennedy Shriver National Institute of Child Health and Human Development, National Institutes of Health, Bethesda, MD, USA

ARTICLE INFO

Handling Editor: Dr. Jasmine Tomar

Keywords:
Influenza
Spike
Membrane
Phosphoinositides
Conservation
Polybasic
Acylation

ABSTRACT

Viral spike proteins mutate frequently, but conserved features within these proteins often have functional importance and can inform development of anti-viral therapies which circumvent the effects of viral sequence mutations. Through analysis of large numbers of viral spike protein sequences from several viral families, we found highly (>99%) conserved patterns within their intracellular domains. The patterns generally consist of one or more basic amino acids (arginine or lysine) adjacent to a cysteine, many of which are known to undergo acylation. These patterns were not enriched in cellular proteins in general. Molecular dynamics simulations show direct electrostatic and hydrophobic interactions between these conserved residues in hemagglutinin (HA) from influenza A and B and the phosphoinositide PIP2. Super-resolution microscopy shows nanoscale colocalization of PIP2 and several of the same viral proteins. We propose the hypothesis that these conserved viral spike protein features can interact with phosphoinositides such as PIP2.

1. Introduction

Viral spike protein sequences are known to mutate, sometimes leading to inefficacy of vaccines or drug resistance (Dharan et al., 2009; Fujisaki et al., 2012; Korber et al., 2020a, 2020b; Obenauer et al., 2006; Plante et al., 2020; Wainright et al., 1991). Because of their involvement in viral binding and entry, spike protein ectodomains have been well characterized (Belouzard et al., 2009; Brelot and Alizon, 2001; Colman and Lawrence, 2003; Floyd et al., 2008; Hamilton et al., 2012; Hoffmann et al., 2020a, 2020b; Ohuchi et al., 2002; Ou et al., 2020; Pabis et al., 2020; Stahelin, 2014; Yang et al., 2004). However, intracellular portions of spike proteins can interact with host cell components and other viral components for trafficking to appropriate locations for assembly and budding (Ali et al., 2000; Barman et al., 2001; Jin et al., 1994, 1997; McCown and Pekosz, 2005; Melikyan et al., 1997; Nayak et al., 2004). Despite the typically small relative size of viral spike intracellular domains (vSIDs), these domains can potentially be anti-viral drug targets.

Anti-viral drug designs which target conserved viral features are highly desirable (Paules et al., 2018). The cytoplasmic tails of some spike proteins have a cysteine-rich motif (Fig. 1). For example, the 10–11 amino acid intracellular domain of hemagglutinin (HA) from influenza A virus (IAV) is known to contain three highly conserved cysteines, C555 (technically within the transmembrane domain), C562, and C565, which can be palmitoylated (Jin et al., 1996, 1997; Naim et al., 1992) or sometimes stearoylated, and whose removal has been shown to alter viral morphology and replication (Chlanda et al., 2017). Site directed mutagenesis has shown that these cysteines are crucial for budding and infectivity, particularly C565 (Chen et al., 2005; Sakai et al., 2002; Wagner et al., 2005; Zurcher et al., 1994). Proper folding of HA in the endoplasmic reticulum (ER) also requires palmitoylation (Blanc et al., 2013). Mutating these final cysteines can inhibit HA fusion activity (Chlanda et al., 2017; Naeve and Williams, 1990), alter viral morphology (Jin et al., 1997), or impair release (Chen et al., 2005), ultimately resulting in a non-infectious virus (Chen et al., 2005; Wagner et al., 2005).

The endodomain of SARS-CoV-1 spike (S) contains 8 cysteines, which are also found in the SARS-CoV-2 S endodomain; the SARS-CoV-2 S endodomain adds a 9th cysteine; these cysteines are acylated and

* Corresponding author.
E-mail addresses: pauline.kamath@maine.edu (P.L. Kamath), benjamin.l.king@maine.edu (B.L. King), samuel.hess@maine.edu (S.T. Hess).
[1] these authors contributed equally.

https://doi.org/10.1016/j.virol.2024.110198
Received 6 June 2024; Received in revised form 23 July 2024; Accepted 31 July 2024
Available online 2 August 2024

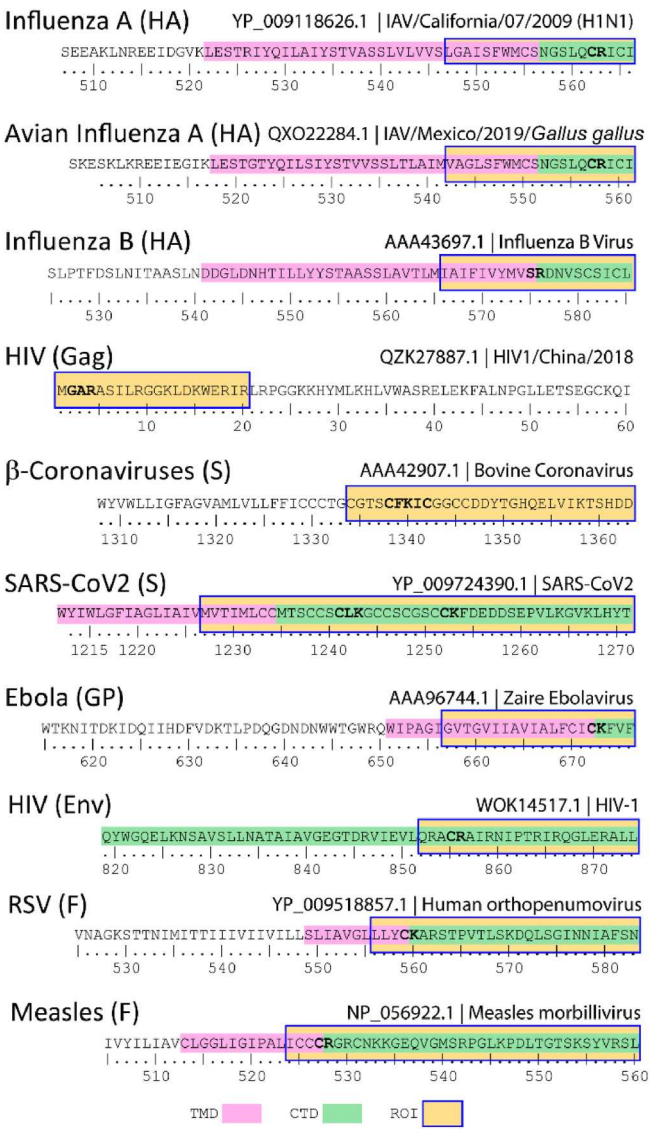

Fig. 1. Representative sequences of cytoplasmic tails (CTDs, green) and transmembrane domains (TMDs, pink) of spike proteins from influenza A virus HA, avian influenza A virus HA, influenza B virus HA, β -coronaviruses S, SARS-CoV-2 S, Ebolavirus GP, HIV Env, RSV F, and Measles F. HIV Gag is shown as a membrane-associated control.The boxed in region of interest (ROI, orange fill with blue outline) indicates the region of the sequence searched for Table 1 patterns.

important for entry (McBride and Machamer, 2010). Cysteines C1234 and C1235 in these coronaviruses must be palmitoylated for S to mediate membrane fusion (Ujike et al., 2012). The severe acute respiratory syndrome coronavirus 2 (SARS-CoV-2) spike (S) protein also catalyzes virus-cell and cell-cell fusion, which are crucial to infection and pathogenesis (Belouzard et al., 2009; Bussani et al., 2020; Hoffmann et al., 2020a; Oprinca and Muja, 2020; Ou et al., 2020; Tang et al., 2020; Wang et al., 2020; Xia et al., 2020; Xu et al., 2020).

Acylated amino acids in close proximity to basic amino acids can control protein interactions with membranes containing phosphoinositides (McLaughlin and Murray, 2005; McLaughlin et al., 2002). Phosphoinositide phosphates (PIPs) mediate a variety of intracellular membrane-associated protein traffic (Altan-Bonnet and Balla, 2012; Balla, 2013; Balla et al., 2012a, b; Di Paolo and De Camilli, 2006; Levin et al., 2017; O'Donnell, 2018; Rozelle et al., 2000). In general, cellular transmembrane proteins are enriched in basic amino acids adjacent to their transmembrane domains (TMDs), typically on the cytoplasmic side (Sharpe et al., 2010). However, viral proteins and interactions with phosphoinositides were not specifically analyzed in this context. Heo et al. (2006) showed that host cell proteins with clusters of basic amino acids and acylated residues could interact with phosphoinositides, which mediated their trafficking to the plasma membrane. *We therefore set out to test whether such amino acid patterns are found in viral intracellular domains, to test whether such features are conserved in viral intracellular domains, and to test whether they are able to interact with host cell phosphoinositides*. Considering that many viral proteins spontaneously form multimers after expression in cells, the number of positive charges found within a spike protein multimer is expected to be comparable to the number found in many PIP-dependent cellular proteins with polybasic residues (Blin et al., 2008; Gambhir et al., 2004; Heo et al., 2006; Lemmon, 2008; McLaughlin and Murray, 2005).

In addition to the conserved cysteines found in vSIDs, interactions between PIPs and viral proteins have been described for human immunodeficiency virus (HIV) (Olety et al., 2015; Ono et al., 2004), Ebolavirus (Gc et al., 2016; Johnson et al., 2016; Kang et al., 2020), SARS-CoV-2 (Raut et al., 2022), and influenza virus (Curthoys et al., 2019; Raut et al., 2022a, 2022b). PIPs play a role in IAV (Fujioka et al., 2013; Hale et al., 2008; Nobs et al., 2016; O'Hanlon et al., 2019; Shin et al., 2007; Zhu et al., 2014; Zhu et al., 2016), SARS-CoV-1 (Chan et al., 2007; Tsoi et al., 2014), and SARS-CoV-2 infection (Bouhaddou et al., 2020; Kang et al., 2020; Yuen et al., 2020). SARS patients showed altered serum levels of PIPs many years after infection (Wu et al., 2017). These interactions are either known or hypothesized to occur through positively charged amino acids in the vSID and the negatively charged phosphoinositide headgroup. In the case of HA, consensus sequences for the vSID show cysteines and positive amino acids adjacent to one another (Veit et al., 2013).

We therefore analyzed the degree to which viral spike proteins contain a particular motif within their vSID: one or more basic amino acids in close proximity to a potentially acylated cysteine, serine, glycine, or hydrophobic amino acid. We abbreviate this generalized feature as (C+/CX+), with the reverse of the features also being included (i.e., +XC or + C). The amino acid sequences queried are shown in Table 1. We chose to analyze a subset of viruses with particular relevance to human health: influenza viruses A and B, with particular attention to avian influenza virus strains, SARS-CoV-2 and other β-coronaviruses, Ebolavirus, HIV1, RSV, and measles. While gag is not technically a spike protein, it does have known interactions with anionic lipid membranes, (Olety et al., 2015; Ono et al., 2004) and is thus of interest. HIV1 envelope protein was also included as a comparison.

We used several approaches: sequence analysis to identify patterns with putative phosphoinositide interaction, all-atom molecular dynamics to test for interactions between phosphoinositides and these residues in viral proteins, and super-resolution microscopy to test for nanoscale interactions between these proteins and phosphoinositides in fixed cells.

2. Material and methods

Sequences were downloaded from the NCBI Virus database (National Library of Medicine N.C.B.I, 1988). in FASTA format and imported into MATLAB using the Bioinformatics Toolbox. Based on published

Table 1
Amino acid patterns searched.

	Forward Sequence	Reverse Sequence
Cysteine Patterns	'CR'	'RC'
	'CK'	'KC'
	'CLK'	KLC'
	'CQK'	'KQC'
	'CIR'	'RIC'
Serine Patterns	'SR'	'RS'
All Other Patterns	'SMQR', 'CFKIC', 'KLH', 'GR', 'GAR'	

information about the cytoplasmic tails of the spike/fusion proteins for these viruses (Cattin-Ortola et al., 2021; Dharan et al., 2009; Gc et al., 2016; Lee and Saphire, 2009; McBride and Machamer, 2010; Ono et al., 2004; Veit, 2012; Veit et al., 2013) the initial 20 aa or final 20–45 amino acids (aa) were analyzed. For influenza A, avian influenza, and influenza B viruses, sufficiently large numbers of sequences were available within the database to allow complete spike (S) protein sequences to be analyzed exclusively. For SARS-CoV-2 sequences, S sequences at least 1260 aa in length were obtained, and the final 45 aa were analyzed. For non-SARS-CoV-2 β-coronaviruses, S sequences at least 1300 aa in length were obtained, and the final 30 amino acids were analyzed. For the control HIV Gag, which is neither a spike nor a transmembrane protein, all available sequences were obtained, and the first 20 aa of the sequence (when complete) were analyzed. For Ebolavirus, envelope glycoprotein (GP) sequences at least 600 aa in length were obtained, and the final 20 aa were analyzed. For HIV Env the final 21 aa were analyzed. For RSV, the final 26 aa from fusion protein sequences were analyzed. For measles, the final 30 aa from fusion protein sequences were analyzed. Any sequences containing missing or ambiguous amino acids were excluded from further analysis. Tail sequences were then searched for the patterns in Table 1. The histogram of location(s) for any patterns found, the relative frequencies of patterns found, and the fraction of sequences containing one or more of the pattern sequences were then calculated.

All Atom Molecular Dynamics. A system containing a solvated membrane bilayer and a trimer of either influenza A HA or influenza B HA was constructed using CHARMM GUI (Jo et al., 2007, 2008, 2009; Lee et al., 2019; Park et al., 2021; Wu et al., 2014). The structure file for HA was obtained from Benton (RCSB 6HJR) (Benton et al., 2018). PyMOL (Schrödinger Inc.) was used to add the cytoplasmic tail domain (CTD) for either influenza A or influenza B to the structure file as it just contained the ectodomain and TMD. The CTD was modeled as an alpha helix which was determined by using AlphaFold (Jumper et al., 2021). We also removed the ectodomain to reduce the number of atoms in our system to improve timings. This modified pdb file was then used to build a bilayer using CHARMM GUI. The cysteines located in the CTD of both Influenza A and Influenza B were palmitoylated in CHARMM GUI. The protein was positioned such that the CTD was just beneath the cytoplasmic leaflet of the plasma membrane (PM) with the TMD inserted in the PM. In the extracellular leaflet of the PM there are 100 cholesterol, 84 DSM, 90 DOPC, and 10 DOPE. The cytoplasmic leaflet contains the following lipids (CHARMM GUI notation): 100 cholesterol, 42 DSM, 45 DOPC, 40 DOPE, 10 DOPS, and 24 SAPI. Na^+ and Cl^- ions were used to neutralize the systems and create a NaCl concentration of 150 mM. The CHARMM36m forcefield was used and water is modeled with TIP3. The pressure and temperature for equilibration of the systems is 1 atm and 310 K.

Creation of Expression vector for Dendra2-tagged Influenza B HA. The expression vector for HA (Influenza B/Victoria/504/2000) was constructed to fuse the HA with Dendra2 at the N-terminal of the HA (Dendra2-HA) using previously published methods (Curthoys et al., 2019; Gurskaya et al., 2006). The DNA for HA Influenza B (codon optimized) was purchased from Sino Biological (Wayne, PA).

Super-Resolution Microscopy. To further test the hypothesis that viral spike proteins can interact with host cell phosphoinositides, we used localization-based super-resolution microscopy (FPALM) (Hess et al., 2006) to visualize spatial distributions of viral proteins and phosphoinositides.

NIH3T3 fibroblast cells were cultured as described in Gudheti et al. (2013); Gudheti et al. (2013). Cells were transfected using lipofectamine 3000 (Invitrogen) with constructs Dendra2-HA and PAmKate-PH. Transfection proceeded at 37 °C/5% CO_2 for 36–44 h in 35 mm MatTek dishes (35 mm, coverglass diameter 20 mm). Images were fixed using 4% PFA in PBS at room temperature.

Two-color super-resolution imaging and localization follow previously published methods (Curthoys et al., 2019; Gunewardene et al., 2011; Hess et al., 2006). A convex lens (f = +350 mm, Newport Corporation) was used to focus a 558 nm laser (CrystalLaser LC, CL558-100) and a 405 nm laser (FBB-405-050-FSFS-100; RGBlase LLC, Fremont, CA) into the back of an inverted microscope (IX71, Olympus) and directed through a 50 x 1.45 NA oil TIRF objective lens (Olympus). Powers of ~17 mW and ~9.5 μW were used for the 558 nm laser and 405 nm laser respectively, with average intensities of 4.4 kW/cm^2 and 0.0025 kW/cm^2. Fluorescence emission from activated probes was captured through the same objective, passed through a quad band dichroic (Di01R 405/488/561/635 nm, Semrock) and a series of notch filters at wavelengths 561 nm (x2) and 405 nm (Stopline, Semrock). Emissions then passed through a 2x telescope (lenses of f = +200 mm and f = +400 mm, Newport Corporation) and were split by a dichroic (FF580-FDi01, Semrock) angled at 34° to achieve a cutoff wavelength of ~600 nm. This split the light into two channels, which were filtered by bandpass filters (ET585/40m, Chroma) and (ET605/70m, Chroma) for the green and red channels respectively. This optical path resulted in a measured camera pixel size equivalent to 119 nm at the sample. For each acquired ROI, image stacks of 10,000 frames were captured using an EMCCD (iXon + DU897DCS-BV, Andor Scientific) with an EM gain of 200 and exposure time of 0.0303 s per frame. Standard localization methods via MATLAB (Mathworks Inc.) were utilized. This included temporal median background subtraction (Piccardi, 2004), intensity based localization thresholding, 2D Gaussian fitting, fit tolerancing, and rendering (Curthoys et al., 2019; Gudheti et al., 2013).

Clusters of PIP2 and HA from influenza B virus were identified using a grid-based density plot as previously described (Curthoys et al., 2019). Grids were binned into 10 nm × 10 nm pixels over the range of the image. Clusters were determined using a 4x density threshold relative to cell average. Clusters were required to have a minimum of 10 identified molecules to filter out false clusters. A radial distribution function (RDF) which plotted the distribution of Dendra2-HA molecules radially from the center of mass of each cluster was generated from the average RDFs across clusters and cells in a given dataset. Similarly, the distribution of PAmKate-PH molecules around the centers of Dendra2-HA clusters were plotted with bleed-through correction to measure colocalization between the species.

3. Results

Examples of viral sequences for each type are shown in Fig. 1. The fraction of viral sequences containing the searched patterns is shown in Table 2. Most of the viral sequences showed one or more patterns frequently.

A high frequency of CR, RC, RIC, and CQK sequences were found in IAVs (Figs. 2 and 3). However, avian IAV strains have virtually no CQK sequences, and a higher fraction of sequences with CR than in IAV generally. In contrast, influenza B virus strains have SR in virtually all of their vSIDs. HIV Gag had a majority of sequences with GAR and GR, which was uncommon among other strains we have analyzed.

Table 2
Fraction of sequences containing C+/CX+.

Virus (Protein)	Matching Sequences	Total Sequences	Percent Matching
Influenza A virus (HA)	91227	91346	99.87
Avian influenza A virus (HA)	13769	13784	99.89
Influenza B virus (HA)	18189	18245	99.69
HIV (Gag)	4306	4402	97.819
β-coronaviruses (S) not including SARS-CoV-2	669	669	100.00
SARS-CoV-2 (S)	899392	899392	100.00
Ebolavirus (GP)	166	166	100.00
HIV (Env)	1818	5517	32.95
RSV (F)	10135	10211	99.26
Measles morbillivirus (F)	961	976	98.46
Uniprot (Non-Viral)	134447	563201	23.87
Random 20mers	285537	1000000	28.55

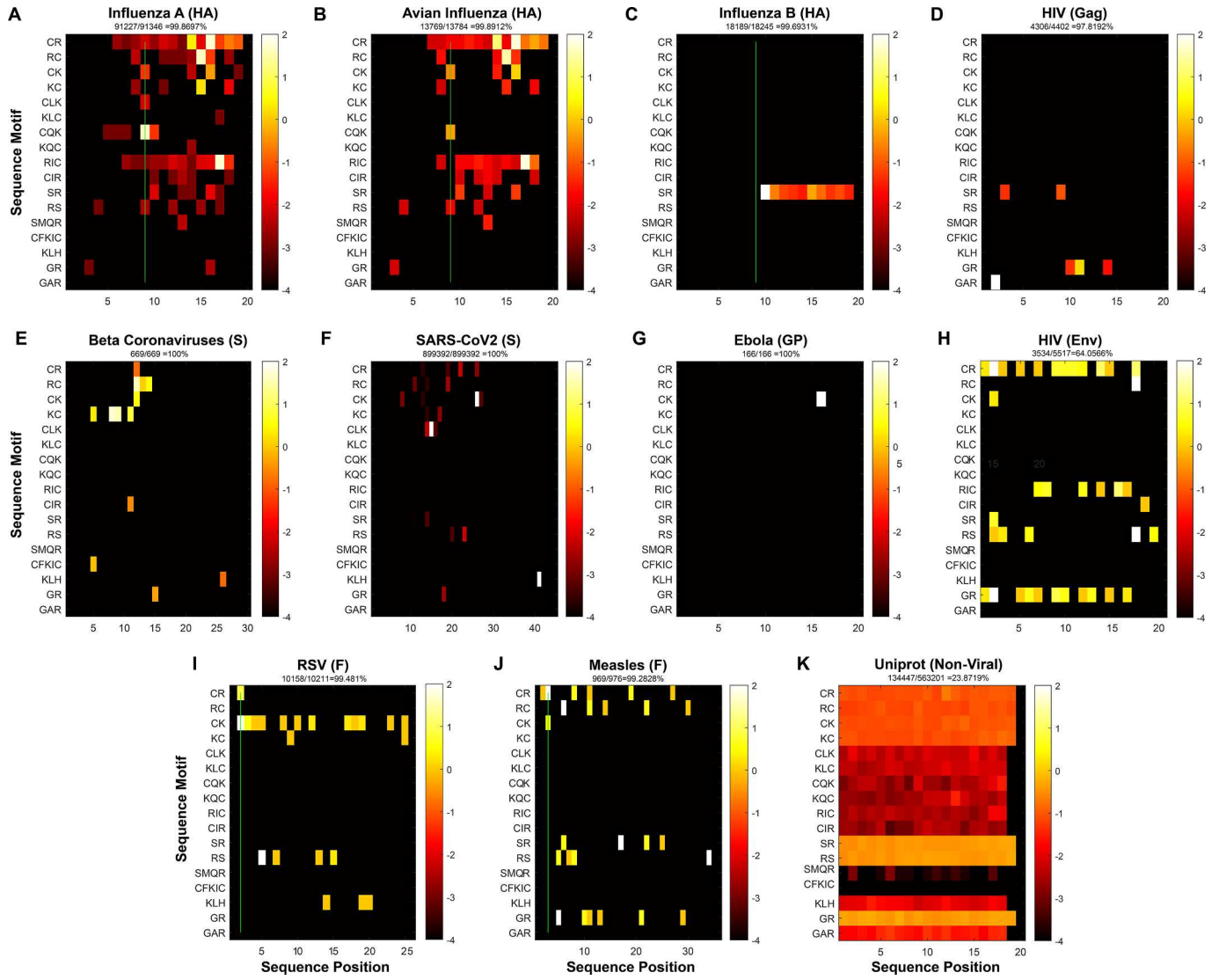

Fig. 2. Frequency distribution of sequence elements as a function of position within the amino acid sequence. The frequency of virus vSID sequences containing each motif is shown as a function of sequence position (higher numbers are toward the carboxy terminal) for **(A)** HA from influenza A virus, **(B)** HA from avian strains of influenza A virus, **(C)** HA from influenza B virus, **(D)** Gag from HIV, **(E)** S from β-coronaviruses *not including SARS-CoV-2*, **(F)** S from SARS-CoV-2, **(G)** GP from Ebolavirus, **(H)** Env from HIV, **(I)** F from RSV, **(J)** F from measles, and **(K)** the final 20 amino acids of proteins within the Uniprot database, each normalized by the total number of sequences. For influenza viruses, RSV, and measles, the approximate location of the junction between transmembrane domain and cytoplasmic tail domain is indicated with a green line. For influenza, coronaviruses, HIV Env, RSV, measles, and Ebola strains, the final (C-terminal) 20–40 amino acids were quantified, respectively (larger values are C-terminal). For HIV Gag the N-terminal 20 amino acids were quantified (1 is the N terminus of the sequence). The pseudo color logarithmic scale shows the relative frequency of sequences (in percent) and the numerical value to the right of the color bar indicates the $\log_{10}$ of the percentage of sequences.

Coronaviruses, in contrast, incorporate cysteines together with lysines more frequently than arginines; SARS-CoV-2 contains CK and CLK but not CR, RC, or any other of our combinations containing R. Furthermore, SARS-CoV-2 contains KLH with a very high frequency, in contrast to all of the other strains presented here. Ebolavirus, on the other hand, shows purely CK, and none of the other sequences. HIV Env shows CR in the position highlighted in Fig. 1 in about ~30% of searched sequences, however other sequences show the C replaced by F, G, W, or other amino acid in the same position.

We also quantified the frequencies of motifs observed in random amino acid sequences, using the published overall rates of amino acids within human proteins (Shemesh et al., 2010). The frequencies of these motifs were spatially uniform (data not shown); the overall frequencies of the motifs can be compared to the other groups (Fig. 3).

As a control, representative viral spike tail sequences from influenza A HA (Q71C80), influenza B HA (P03460), HIV Gag (P12493), HA from avian IAV (P03452), Ebola (Q05320), Zika (Q32ZE1), β-Coronavirus (K9N5Q8), and SARS-CoV-2 (P0DTC2) were analyzed with Multiple Expectation maximizations for Motif Elicitation (MEME) (Bailey et al., 2015). Individual motifs were then submitted to a Tomtom (Gupta et al., 2007) search using the PROSITE and ELM2018 databases. No matches were found for any motif in the databases - the lowest E-value found was 0.11. A random representative sample of all of the viral tail sequences was then combined into a single file and submitted to MEME. No motifs were identified. Single tail sequences from each virus were then submitted to an InterPro search. Although viral sequences were identified as viral in origin, none matched any other known domains.

To further investigate patterns surrounding cysteine near the TMD/CTD junction, amino acids ±3 spaces from the first C in the tail were analyzed from HA from influenza A virus, HA from avian strains of influenza A virus, HA from influenza B virus, Env from HIV, S from β-coronaviruses *not including SARS-CoV-2*, S from SARS-CoV-2, GP from

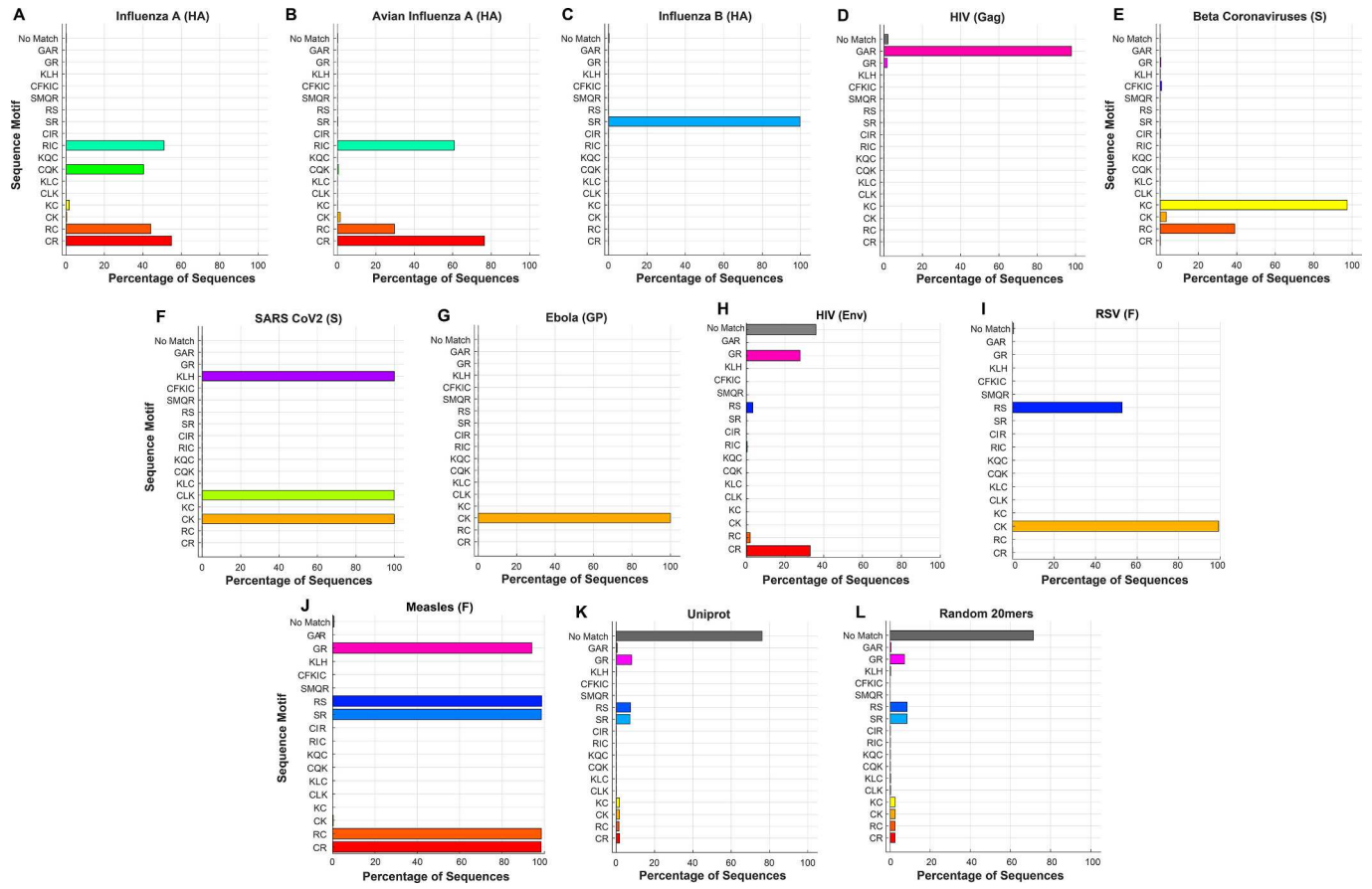

Fig. 3. Frequency histograms of sequence motifs as a function of virus type. The percentage of virus vSID sequences containing each motif is shown in **(A)** HA from influenza A virus, **(B)** HA from avian strains of influenza A virus, **(C)** HA from influenza B virus, **(D)** Gag from HIV, **(E)** S from β-coronaviruses *not including SARS-CoV-2,* **(F)** S from SARS-CoV-2, **(G)** GP from Ebolavirus, **(H)** Env from HIV, **(I)** F from RSV, and **(J)** F from Measles, **(K)** the final 20 amino acids of proteins within the Uniprot database, **(L)** randomly generated 20mers using the overall frequency of amino acids in human proteins, each normalized by the total number of patterns found for the given virus. The total number of matches and the total number of sequences analyzed for the given virus type are shown in Table 2.

Ebolavirus, F from RSV, and F from measles. The positions of the first cysteine in the tails of each of the sequences was obtained from Veit (2012). If a C was found in the exact position, the amino acid neighbors were counted. If not, that sequence was skipped. The total count for each amino acid at each position was then normalized by the expected amino acid distribution from Shemesh et al. (2010); Shemesh et al. (2010). The results are shown in Fig. 4. As a control, non-viral Uniprot sequences were searched with the same methodology, and the results in Fig. 4J show an expected average distribution. This analysis confirms the C+/CX + patterns that were searched for from Table 1 and highlights some other patterns such as CN in measles (Fig. 4I). Sequence logos were also created using the Bioinformatics Toolbox in MATLAB (Mathworks Inc.) and are shown below each panel of the corresponding protein in Fig. 4. These logos were created directly from the sequence data (only sequences with C in the exact position searched for) and are not normalized by expected amino acid distribution.

Molecular Dynamics (MD) Simulations. All-atom MD simulations were conducted so that any interaction between influenza HA and phosphoinositides could be observed at the molecular level and the mechanism of interaction tested. Two MD simulations were progressed to 1 μs containing either HA from IAV (HA_A) in a mammalian PM membrane or HA from influenza B (HA_B) in a mammalian PM membrane. Both systems were minimized and equilibrated accordingly. The amount of PIP2 in the cytoplasmic leaflet was increased so that there can be a chance of HA and PIP2 interacting within the simulated timescale. The interactions were quantified through RDF calculations using the arginines in the CTD of HA and the phosphates in the PIP2 headgroup. Both HA_A and HA_B have a spike within 1 nm showing an increase of PIP2 density close to the CTD of HA. HA_B has a much higher peak than HA_A. Both RDFs decrease after 1 nm and slowly approach 1 for $r > 1$ nm. The results are shown in Fig. 5.

Super-Resolution Microscopy. To further test the hypothesis that viral spike proteins can interact with phosphoinositides, we followed up on our published findings showing interaction between influenza A HA and PIP2 (Curthoys et al., 2019) and SARS-CoV2 spike and PIP2 (Raut et al., 2022b). Fig. 6 shows super-resolution imaging of influenza B spike protein tagged with photoconvertible fluorescent protein Dendra2 (HA_B-Dendra2) alongside the PH-PAmKate, the pleckstrin homology PIP2-binding domain tagged with a PAmKate label (Curthoys et al., 2019) compatible with super-resolution microscopy (Gunewardene et al., 2011). Colocalization patterns of Dendra2-HA_B and PAmKate-PH are observed (Fig. 6) and quantified using the radial distribution function (RDF) (see methods). Compared to HA from influenza A (HA_A), the influenza B HA (HA_B) appears to form denser, more compact clusters as quantified by the width and height of the peak in the RDF (Fig. 6B) compared with similar analysis for HA_A in (Curthoys et al., 2019). Bleed-through corrected data (10% bleed-through used for each channel) supports the visual observation of PIP2 clustering around this protein with density peaking around 100 nm from the center of the HA clusters and persisting for around 500 nm.

4. Discussion

Acylation of viral proteins is fairly common (Gadalla et al., 2020;

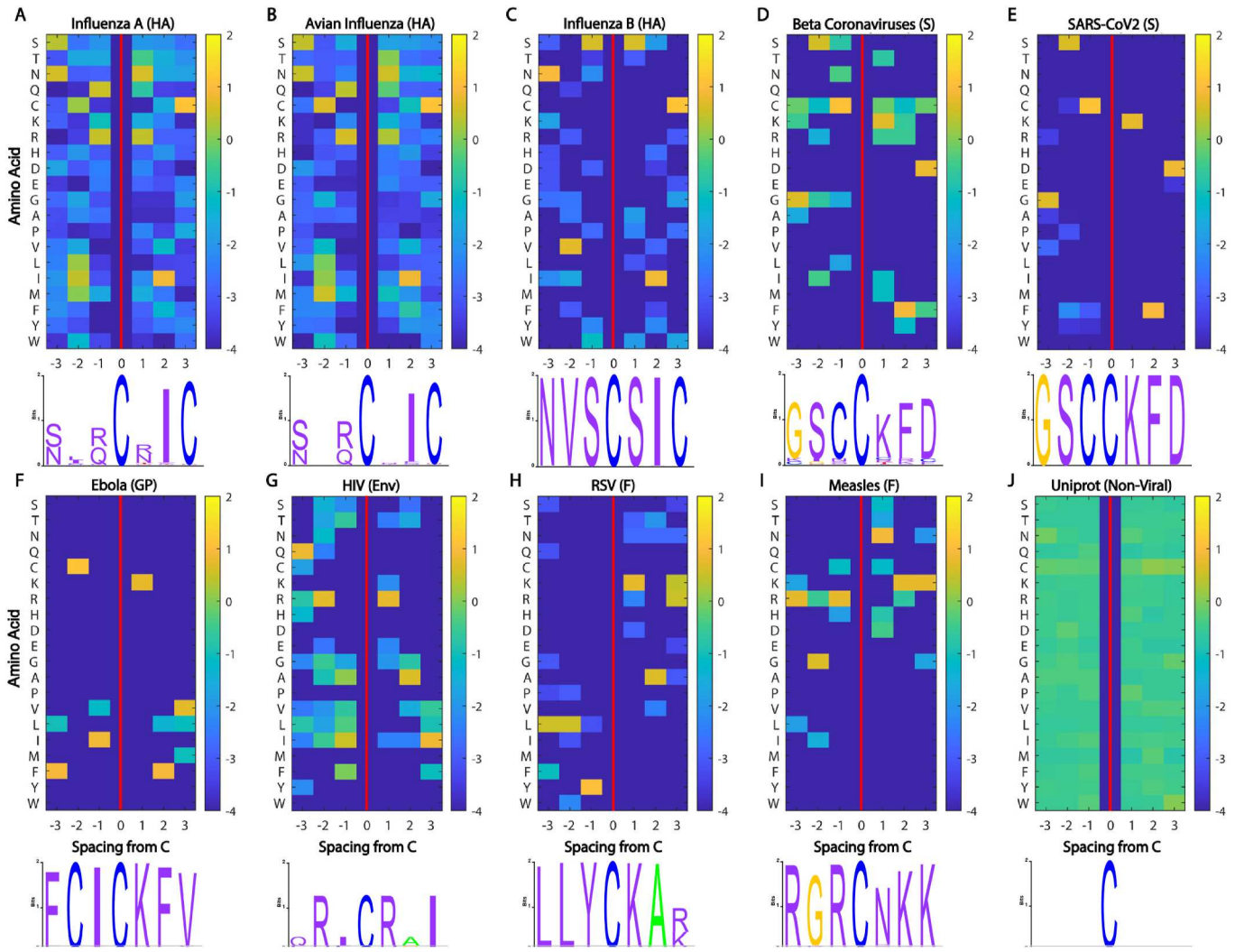

Fig. 4. Frequency histograms of amino acid neighbors to the first cysteine in the CTD as a function of virus type. The red line at the 0 position on each histogram shows the position of Cys, and the spacing searched was up to 3 away from Cys in both directions. The amino acids on the y-axis are organized by properties, with roughly polar amino acids towards the top and non-polar towards the bottom. The sequences analyzed were from **(A)** HA from influenza A virus, **(B)** HA from avian strains of influenza A virus, **(C)** HA from influenza B virus, **(D)** S from β-coronaviruses *not including SARS-CoV-2*, **(E)** S from SARS-CoV-2, **(F)** GP from Ebolavirus, **(G)** Env from HIV, **(H)** F from RSV, **(I)** F from measles, **(J)** the Cys at position 3 into the final 20 amino acids of proteins within the Uniprot database. The pseudocolor logarithmic scale shows the relative frequency of amino acids normalized by expected distribution (Shemesh et al., 2010) in percent, and the numerical value to the right of the color bar indicates the $\log_{10}$ of the percentage of sequences. Sequence logos (not normalized by expected distribution) are shown below each panel. Note this analysis includes only the first cysteine in the CTD, although other CTD cysteines do sometimes contain similar patterns.

Gadalla and Veit, 2020; Ito et al., 2001) and in some cases conserved (Veit et al., 2013), but the role played by acylation in the viral life cycle is not always clear. Influenza HA and SARS-CoV-1 S are acylated at highly-conserved cysteines (McBride and Machamer, 2010; Veit et al., 2013). Myristoylation of HIV-Gag is required for production of infectious particles (Furuishi et al., 1997), and the saturation of the PIP acyl chains mediates the interaction with Gag (Olety et al., 2015). Trafficking of host cell proteins to the plasma membrane is mediated by polybasic amino acids and acylation through interaction with phosphoinositides, specifically PIP2 (Heo et al., 2006). In a number of viral spike proteins, we find conservation of certain motifs which combine basic amino acids and cysteines or serines. The high level of conservation suggests these motifs are key in viral functioning.

A number of viral proteins interact with phosphoinositides. HIV Gag is known to interact with PIP2 (Olety et al., 2015; Ono et al., 2004), and the Ebola VP40 interacts directly with PIP2 (Gc et al., 2016). Influenza HA and SARS-CoV-2 S both interact with PIP2 (Curthoys et al., 2019; Raut et al., 2022, 2022a), and influenza virus M1 assembly with HA is mediated by PIP2 (Raut et al., 2022a). We hypothesize that this interaction occurs between PIP2 and the HA CTD in the case of influenza, and between PIP2 and the S endodomain in the case of SARS-CoV-2. Experimental data from our study show that multiple viral spike proteins interact with PIP2: HA from IAV (Curthoys et al., 2019), SARS-CoV-2 Spike (Raut et al., 2022b), and HA from influenza B virus (Fig. 6), supporting this hypothesis. All-atom MD simulations show direct interaction between arginines in the HA CTD and phosphate groups in the PIP2 head group, also supported/stabilized by acylated cysteines in the influenza A HA CTD (Fig. 5A–B) and in the influenza B HA CTD (Fig. 5C–D), resulting in a net enrichment of PIP2 near HA (Figs. 5 and 6). The relative generality of this finding is to some extent demonstrated by the experimental and molecular dynamics evidence shown in multiple viral spike proteins by multiple methods.

The vast majority of viral spike proteins analyzed contain at least one of the C+/CX + sequence elements; strikingly, more than 99% of all influenza virus, coronavirus, Ebolavirus, and RSV strains contained one or more of these elements (Figs. 2 and 3; Table 2). Measles virus strains contain C+/CX+ in more than 98% of searched sequences. While HIV Gag sequences preferentially contain the GAR pattern at the N-terminus

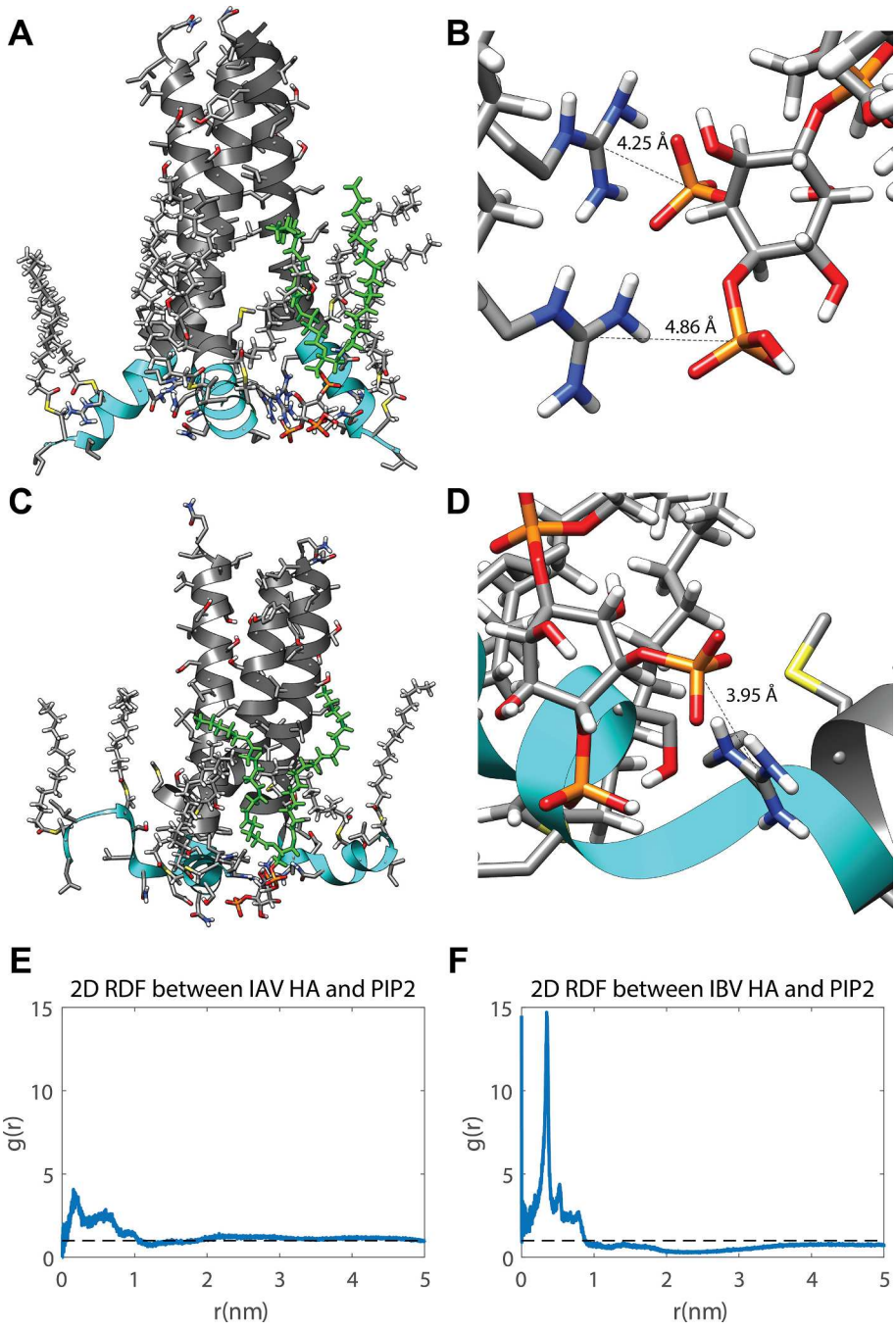

Fig. 5. **(A)** Snapshot of an all-atom MD simulation of IAV HA (HA_A) interacting with PIP2 in a solvated membrane bilayer (other lipids not shown). The HA-CTD is colored cyan and the HA-TMD is colored gray. **(B)** Zoomed in view of the interactions showing the phosphates in the head group of PIP2 interacting with the two arginines located in the CTD of IAV HA. The dashed lines represent the distances between the two phosphates in the PIP2 headgroup and the CZ atom on Arg-557 and Arg-561. **(C)** Snapshot of an all-atom MD simulation of HA from Influenza B (HA_B) interacting with PIP2. The CTD is colored cyan and the TMD is colored gray. **(D)** Zoomed in view showing the headgroup of PIP2 interacting with the arginine in the CTD of HA_B. The dashed line shows the distance between a phosphate on the headgroup of PIP2 and the CZ atom of Arg-576. **(E–F)** RDF measurements between the Arg and the headgroups of PIP2 for both HA_A and HA_B.

of gag, it is known that this glycine is myrisytoylated (Pal et al., 1990), and that the arginine interacts with PIP2 (Olety et al., 2015; Ono et al., 2004), thus recapitulating the overall pattern of an acylated residue close to a PIP-interacting basic residue. Interestingly, gag preferentially interacts with PIP2 containing unsaturated lipid tails (Olety et al., 2015). In HIV Env, these sequences are not as highly conserved. While about 64% of sequences contain a CR or GR pattern, both of which are commonly acylated, the rest of the sequences contain Phe or Trp. While Trp can sometimes be acylated (Hu et al., 2022), neither Phe or Trp are commonly acylated, and thus may not represent substitutes for C or G. We do not know why 36% of the HIV Env sequences do not contain the expected patterns. In contrast, the Uniprot database, which includes many cellular proteins, showed a much lower frequency of the motifs (23.87%). Furthermore, 100% of β-coronavirus, SARS-CoV-2, and Ebolavirus sequences showed at least one of the motifs. Considering the large number of SARS-CoV-2 sequences analyzed (more than 899,000), this is a remarkable level of conservation. The avian IAV strains show a similar distribution of the sequences compared to all IAV.

In contrast, the influenza B virus strains all have the SR motif (99.693%), or do not contain any of the C+/CX + elements (0.307%).

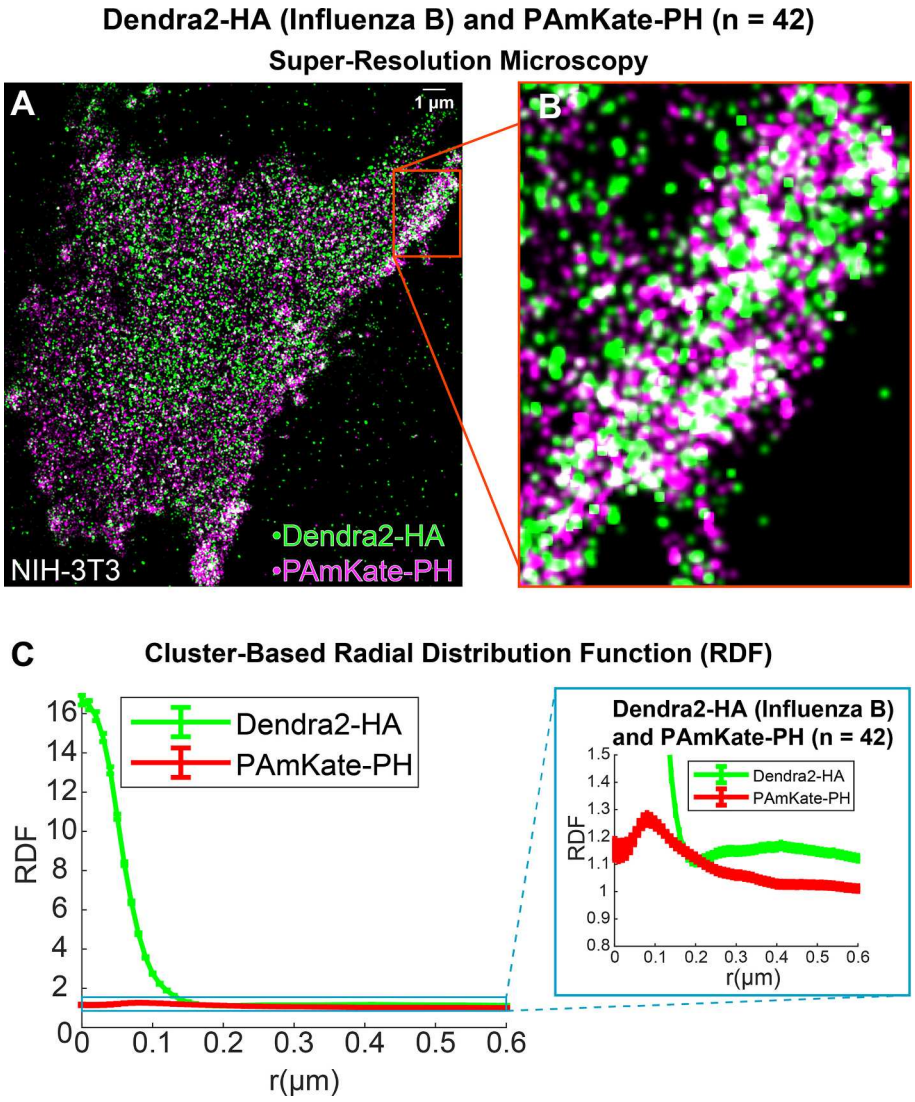

Fig. 6. **(A)** Representative image of Dendra2-HA (green) from influenza B virus and PAmKate-PH (magenta) in fixed NIH-3T3 cell captured using TIRF-FPALM. Colocalized regions can be seen in white. Co-clustering can be seen along the right edge of the cell. **(B)** Density around HA clusters is quantified for HA (green) and for PAmKate-PH (red) as averaged over 42 cells collected from three replicates. Average density of HA clusters is seen to be ~17x the cell average at the center and maintains a density greater than 4x the cell average until 80 ± 10 nm. PAmKate-PH can be seen to co-cluster with Dendra2-HA with highest density ~100 nm from the center of the cluster.

While this result is somewhat unexpected since cysteines are commonly acylated (Blanc et al., 2013; Li et al., 2022; Linder and Deschenes, 2007), serines may also be acylated (Doubravska et al., 2011; Fu and Xiang, 2015; Port and Basler, 2010; Takada et al., 2006). Fig. 5C–D demonstrates that Influenza B HA (HA_B) does interact with PIP2, even in the absence of palmitoylation. Based on results for HA from influenza A, the palmitoylation contributes to the interaction (Fig. 5A and B). Thus, if the Ser in the SR motif is acylated, this would be expected to further strengthen the interaction between PIP2 and HA_B.

Comparison of the observed frequency of no matching motif in random 20mers (71.44%) and Uniprot database sequences (76.13%) shows somewhat lower motif frequencies in actual proteins than in random sequences. The observed frequencies of SR (8.44%) and RS (8.44%) are higher than CR (2.47%) and RC (2.45%) in the random 20mers (Fig. 3J). This relative pattern is reproduced qualitatively in the analysis of Uniprot sequences SR (7.24%) and RS (7.49%), which are again higher than CR (1.85%) and RC (1.49%). However, the overall frequency of motifs is somewhat higher in the random 20mers, and the sequence order seems to play a role in motif frequencies in the Uniprot and viral sequences, where in the random sequences it does not, as expected. One explanation for the differences in CR vs RC observed in many sequence types (Fig. 3) is the potential for affinity for membranes when the cysteine is acylated; the order of residues might be biased by the location of transmembrane (hydrophobic) and hydrophilic residues relative to any given cysteine, on average. For example, if the Cys is close to the transmembrane domain (TMD)-CTD junction, placing the Arg N terminal to the Cys could, in some circumstances, force the Arg side chain to reside within the bilayer, an energetically unfavorable situation. Perhaps some of the bias of Cys-Arg over Arg-Cys comes from this possibility. However, the observed frequencies of RC vs CR and KC vs CK do not show this preference in general (Fig. 3).

The differences in SR/RS compared to CR/RC motif frequencies in random 20mers is likely due to the higher overall frequency of Ser compared to Cys in human proteins. This pattern is also observed in the Uniprot sequences. However, the SR/RS frequencies are in general quite low except in influenza B viruses, again suggesting that overall amino acid frequencies do not explain these patterns.

Are these conserved motifs also generally used for interaction with PIP2 or other phosphoinositides? We hypothesize that the high level of conservation of C+/CX + elements within a wide variety of viral spike

intracellular domains (vSIDs) suggests a function for these domains, and that their purpose is to enhance membrane association of the vSID, and interact with phosphoinositides through electrostatic and hydrophobic interactions. One possible connection to infection is through viral assembly, whereby interactions between viral membrane proteins and phosphoinositides could mediate trafficking of viral proteins to the assembly site(s). Furthermore, the particles which assemble, bud, and are released must contain the proper distribution of viral membrane proteins in order to achieve binding to and entry into a subsequent host cell. Interactions between the viral membrane proteins and phosphoinositides during assembly are likely to modulate the spatial arrangement and membrane properties of subsequently released particles. Since high-density clustering of viral spike proteins has been previously related to binding and entry through membrane fusion (Chen et al., 2020; Ellens et al., 1990a; Takeda et al., 2003; Zhang et al., 2020), we suggest that the C+/CX + elements could play a role in the clustering of viral membrane proteins and therefore their ability to enable binding and entry, and their co-clustering with other viral components for assembly. We hypothesize that these elements are conserved because they are involved in these aspects of the viral life cycle. Future work will need to test these hypotheses more thoroughly and explore their generality.

Several alternate hypotheses could also explain the observed conservation of these sequence elements. **The sequences could relate to acyltransferase function.** One known sequence for palmitoyl acyltransferases is the DHHC motif (Ohno et al., 2006; Woodley and Collins, 2021). It is known that HA from influenza A virus can be acylated by several ZDHHCs, but not HA from influenza B or C (Gadalla et al., 2020). While this could help explain the remarkable conservation of the cysteines in the HA CTD (Veit et al., 2013), it is not clear how a nearby basic residue would be involved, or why they would be conserved. Nonetheless, these enzymes may serve as promising anti-viral drug targets (Gadalla and Veit, 2020).

The CaaX sequence is also known to encode post-translational modification of proteins with geranyl-geranyl or farnesyl groups, among a number of others, and also to encode C-terminal cleavage of the protein after the Cys (Krishnankutty et al., 2009). However, the features observed here (Table 1) do not fit this pattern in general, and searching of the viral sequences for 22 CXXX motifs presented in the literature (Berger et al., 2022) yielded only a single hit 1/91346 influenza a sequences, zero for all other viral sequences, and 753/563201 positive results for uniprot non-viral sequences. Similarly for the sequence CKQQ, which is also involved in post-translational modification of proteins (Berger et al., 2022), we found zero instances within viral sequences examined, but 47 instances within the Uniprot non-viral sequences. Searches for a variety of protein sequence motifs using MEME and Tomtom did not find any matches (based on E-value<0.1) to these or related motifs within the viral protein sequences examined.

The motifs could direct the structure and the architecture of the cytoplasmic tails. This hypothesis is certainly reasonable and could be true at the same time that the motifs also mediate phosphoinositide interactions. In fact, the presence of a phosphoinositide interacting with the HA CTD seems to elicit a specific structure of the CTD (Fig. 5). It would be very interesting to do MD simulations of several other viral membrane proteins containing this motif to test for and compare their interactions with phosphoinositides.

The motifs could control interactions with other viral membrane proteins in viral assembly. It has been hypothesized that the palmitoylated cysteines in the HA CTD mediate HA-HA clustering and interactions between HA, NA and M1, although this issue remains somewhat controversial (Chen et al., 2005; Chlanda et al., 2017; Jin et al., 1994, 1997; Veit et al., 2013). The cysteines in the HA CTD are certainly important for several aspects of the influenza virus life cycle; mutation of the final HA CTD cysteine inhibits growth of the virus (Chlanda et al., 2017). Yet, the role of the basic amino acid(s) nearby has not been extensively investigated. Also, it is worth pointing out that in HA sequences, the positive amino acid is found *either* directly prior to or directly after one of the CTD cysteines or serines, suggesting that the sequence order does not matter. This particular observation eliminates certain sequence-dependent kinds of interactions. We therefore argue that the hypothesis that basic amino acids work together with acylated cysteines in a non-specific electrostatic + hydrophobic interaction with PIP2 is a distinct and useful hypothesis for further investigation.

To test whether PIP2 can interact with HA and M1, we used super-resolution microscopy and found that it does (Curthoys et al., 2019; Raut et al., 2022a). We also tested whether HA-M1 interactions were dependent on PIP2 and found that they are (Raut et al., 2022a). Compounds which modulated PIP2 within the plasma membrane were also found to modulate influenza A virus infectivity (Raut et al., 2022b). These experimental results already demonstrate a role for certain phosphoinositides in influenza virus assembly. The findings that HA from influenza B (Fig. 6) and SARS-CoV-2 S colocalize with PIP2 (Raut et al., 2022) are consistent with the hypothesis that phosphoinositides could interact with a wide variety of viral membrane proteins.

In normal cells, PIP2 can medate trafficking of proteins with polybasic residues and acylated cysteines to the plasma membrane (Heo et al., 2006). We propose that viruses may use these sequence motifs to "hijack" phosphoinositide-dependent host cell functions to enable or enhance infection. Further work is needed to clarify the roles these sequence motifs might play in the viral life cycle. Considering that high-density membrane clustering of HA is needed for viral entry through HA-dependent membrane fusion (Ellens et al., 1990b; Takeda et al., 2003) and HA cluster density is dependent on PIP2 (Curthoys et al., 2019; Raut et al., 2022a, 2022b), there could be a link between HA clustering, PIP2, and viral entry, but this has yet to be tested. An exciting recent study shows PIP2 can catalyze vesicle fusion (Ali Moussa et al., 2024), but the connection to viral membrane fusion remains unknown. Palmitoylation of the cysteine residues in the spike protein for both SARS-CoV-1 and SARS-CoV-2 is essential for membrane fusion activity (Ujike et al., 2012; Wu et al., 2021). Considering all SARS-CoV-2 sequences searched contain a Cys motif in the same position suggests there could be a link between the conserved sequences and palmitoylation, and thus spike-catalyzed membrane fusion, on which SARS-CoV-1 and SARS-CoV-2 depend for entry. Again, these ideas need to be further tested. Because of the numerous signaling pathways and cellular functions that PIP2 modulates, there are many ways in which PIP2 could affect viral entry, replication, assembly, and budding. If identified, such involvement could be investigated to identify new anti-viral targets.

Conclusions. We analyzed viral spike proteins from a number of viral families and found that they contain highly conserved sequence features in their cytoplasmic tails, typically consisting of one or more basic amino acids in proximity to one or more cysteines. We hypothesized that these basic amino acids, together with the cysteines, when acylated, could interact with phosphoinositides as many cellular proteins are known to do. Using molecular dynamics simulations, we show that in HA from influenza A and B, these features do interact directly with PIP2 through a combination of electrostatic interactions and association of the acylated cysteines with the PIP2 tails. Experimental evidence from super-resolution microscopy verifies that several of these same spike proteins colocalize with PIP2 at the nanoscale. Taken together, these results are suggestive of a mechanism of interaction between viral spike proteins and host cell phosphoinositides. Further work is needed to test the generality of this proposed mechanism.

Funding

This research was funded by National Institutes of Health Grant R15GM139070 (PI: Hess), and by Institutional Development Awards (IDeA) from the National Institute of General Medical Sciences of the National Institutes of Health under grant numbers P20GM144265 and P20GM103423 (B. King). Supercomputer time was provided by the UMaine Advanced Computing Group, and by National Science Foundation ACCESS award BIO230058 (PI: Hess).

CRediT authorship contribution statement

Vinh-Nhan Ngo: Writing – review & editing, Visualization, Validation, Software, Investigation, Formal analysis, Data curation. **David P. Winski:** Writing – review & editing, Visualization, Validation, Software, Methodology, Investigation, Formal analysis, Data curation. **Brandon Aho:** Writing – review & editing, Visualization, Methodology, Investigation, Formal analysis, Data curation. **Pauline L. Kamath:** Writing – review & editing, Writing – original draft, Methodology, Conceptualization. **Benjamin L. King:** Writing – review & editing, Validation, Methodology, Investigation, Conceptualization. **Hang Waters:** Writing – review & editing, Resources, Methodology. **Joshua Zimmerberg:** Writing – review & editing, Resources. **Alexander Sodt:** Writing – review & editing, Visualization, Validation, Software, Methodology, Investigation, Funding acquisition, Formal analysis, Data curation, Conceptualization. **Samuel T. Hess:** Writing – review & editing, Writing – original draft, Visualization, Validation, Supervision, Software, Resources, Project administration, Methodology, Investigation, Funding acquisition, Formal analysis, Data curation, Conceptualization.

Declaration of competing interest

The authors declare that they have no known competing financial interests or personal relationships that could have appeared to influence the work reported in this paper.

Data availability

Data will be made available on request.

Acknowledgments

We gratefully acknowledge the authors, originating and submitting laboratories that have shared their proteomic data with the UNIPROT database, and viral genomic data with NCBI Virus, which enabled this work. The authors thank Julie Gosse and C.T. Hess for valuable discussions, and Timothy Campbell and Mariana Haletska for technical assistance.

Appendix A. Supplementary data

Supplementary data to this article can be found online at https://doi.org/10.1016/j.virol.2024.110198.

References

Ali, A., Avalos, R.T., Ponimaskin, E., Nayak, D.P., 2000. Influenza virus assembly: effect of influenza virus glycoproteins on the membrane association of M1 protein. J. Virol. 74, 8709–8719.

Ali Moussa, H.Y., Shin, K.C., Ponraj, J., Park, S.H., Lee, O.S., Mansour, S., Park, Y., 2024. PIP2 is an electrostatic catalyst for vesicle fusion by lowering the hydration energy: arresting vesicle fusion by masking PIP2. ACS Nano 18 (20), 12737–12748.

Altan-Bonnet, N., Balla, T., 2012. Phosphatidylinositol 4-kinases: hostages harnessed to build panviral replication platforms. Trends Biochem. Sci. 37, 293–302.

Balla, T., 2013. Phosphoinositides: tiny lipids with giant impact on cell regulation. Physiol. Rev. 93, 1019–1137.

Balla, T., Wymann, M., York, J.D., 2012a. Phosphoinositides I enzymes of synthesis and degradation. Subcellular Biochemistry. Springer, Dordrecht ; New York, p. 352, 1 online resource (xv.

Balla, T., Wymann, M., York, J.D., 2012b. Subcellular Biochemistry. In: Phosphoinositides II the Diverse Biological Functions. Springer, Dordrecht ; New York, p. 1 online resource (xv, 460 pp.).

Barman, S., Ali, A., Hui, E.K.W., Adhikary, L., Nayak, D.P., 2001. Transport of viral proteins to the apical membranes and interaction of matrix protein with glycoproteins in the assembly of influenza viruses. Virus Res. 77, 61–69.

Belouzard, S., Chu, V.C., Whittaker, G.R., 2009. Activation of the SARS coronavirus spike protein via sequential proteolytic cleavage at two distinct sites. Proc. Natl. Acad. Sci. U.S.A. 106, 5871–5876.

Benton, D.J., Nans, A., Calder, L.J., Turner, J., Neu, U., Lin, Y.P., Ketelaars, E., Kallewaard, N.L., Corti, D., Lanzavecchia, A., Gamblin, S.J., Rosenthal, P.B., Skehel, J.J., 2018. Influenza hemagglutinin membrane anchor. Proc. Natl. Acad. Sci. U.S.A. 115 (40), 10112–10117.

Berger, B.M., Yeung, W., Goyal, A., Zhou, Z., Hildebrandt, E.R., Kannan, N., Schmidt, W. K., 2022. Functional classification and validation of yeast prenylation motifs using machine learning and genetic reporters. PLoS One 17, e0270128.

Blanc, M., Blaskovic, S., van der Goot, F.G., 2013. Palmitoylation, pathogens and their host. Biochem. Soc. Trans. 41, 84–88.

Blin, G., Margeat, E., Carvalho, K., Royer, C.A., Roy, C., Picart, C., 2008. Quantitative analysis of the binding of ezrin to large unilamellar vesicles containing phosphatidylinositol 4,5 bisphosphate. Biophys. J. 94, 1021–1033.

Bouhaddou, M., Memon, D., Meyer, B., White, K.M., Rezelj, V.V., Correa Marrero, M., Polacco, B.J., Melnyk, J.E., Ulferts, S., Kaake, R.M., Batra, J., Richards, A.L., Stevenson, E., Gordon, D.E., Rojc, A., Obernier, K., Fabius, J.M., Soucheray, M., Miorin, L., Moreno, E., Koh, C., Tran, Q.D., Hardy, A., Robinot, R., Vallet, T., Nilsson-Payant, B.E., Hernandez-Armenta, C., Dunham, A., Weigang, S., Knerr, J., Modak, M., Quintero, D., Zhou, Y., Dugourd, A., Valdeolivas, A., Patil, T., Li, Q., Huttenhain, R., Cakir, M., Muralidharan, M., Kim, M., Jang, G., Tutuncuoglu, B., Hiatt, J., Guo, J.Z., Xu, J., Bouhaddou, S., Mathy, C.J.P., Gaulton, A., Manners, E.J., Felix, E., Shi, Y., Goff, M., Lim, J.K., McBride, T., O'Neal, M.C., Cai, Y., Chang, J.C.J., Broadhurst, D.J., Klippsten, S., De Wit, E., Leach, A.R., Kortemme, T., Shoichet, B., Ott, M., Saez-Rodriguez, J., tenOever, B.R., Mullins, R.D., Fischer, E.R., Kochs, G., Grosse, R., Garcia-Sastre, A., Vignuzzi, M., Johnson, J.R., Shokat, K.M., Swaney, D. L., Beltrao, P., Krogan, N.J., 2020. The global phosphorylation landscape of SARS-CoV-2 infection. Cell 182, 685–712 e619.

Brelot, A., Alizon, M., 2001. HIV-1 entry and how to block it. Aids 15, S3–S11.

Bussani, R., Schneider, E., Zentilin, L., Collesi, C., Ali, H., Braga, L., Volpe, M.C., Colliva, A., Zanconati, F., Berlot, G., Silvestri, F., Zacchigna, S., Giacca, M., 2020. Persistence of viral RNA, pneumocyte syncytia and thrombosis are hallmarks of advanced COVID-19 pathology. EBioMedicine 103104.

Cattin-Ortola, J., Welch, L.G., Maslen, S.L., Papa, G., James, L.C., Munro, S., 2021. Sequences in the cytoplasmic tail of SARS-CoV-2 Spike facilitate expression at the cell surface and syncytia formation. Nat. Commun. 12, 5333.

Chan, C.M., Ma, C.W., Chan, W.Y., Chan, H.Y., 2007. The SARS-Coronavirus Membrane protein induces apoptosis through modulating the Akt survival pathway. Arch. Biochem. Biophys. 459, 197–207.

Chen, B.J., Takeda, M., Lamb, R.A., 2005. Influenza virus hemagglutinin (H3 subtype) requires palmitoylation of its cytoplasmic tail for assembly: M1 proteins of two subtypes differ in their ability to support assembly. J. Virol. 79, 13673–13684.

Chen, Y.C., Sood, C., Marin, M., Aaron, J., Gratton, E., Salaita, K., Melikyan, G.B., 2020. Super-resolution fluorescence imaging reveals that serine incorporator protein 5 inhibits human immunodeficiency virus fusion by disrupting envelope glycoprotein clusters. ACS Nano 14, 10929–10943.

Chlanda, P., Mekhedov, E., Waters, H., Sodt, A., Schwartz, C., Nair, V., Blank, P.S., Zimmerberg, J., 2017. Palmitoylation contributes to membrane curvature in influenza A virus assembly and hemagglutinin-mediated membrane fusion. J. Virol. 91.

Colman, P.M., Lawrence, M.C., 2003. The structural biology of type I viral membrane fusion. Nat. Rev. Mol. Cell Biol. 4, 309–319.

Curthoys, N.M., Mlodzianoski, M.J., Parent, M., Butler, M.B., Raut, P., Wallace, J., Lilieholm, J., Mehmood, K., Maginnis, M.S., Waters, H., Busse, B., Zimmerberg, J., Hess, S.T., 2019. Influenza hemagglutinin modulates phosphatidylinositol 4,5-bisphosphate membrane clustering. Biophys. J. 116, 893–909.

Dharan, N.J., Gubareva, L.V., Meyer, J.J., Okomo-Adhiambo, M., McClinton, R.C., Marshall, S.A., George, K.S., Epperson, S., Brammer, L., Klimov, A.I., Bresee, J.S., Fry, A.M., 2009. Infections with oseltamivir-resistant influenza A(H1N1) virus in the United States. JAMA, J. Am. Med. Assoc. 301, 1034–1041.

Di Paolo, G., De Camilli, P., 2006. Phosphoinositides in cell regulation and membrane dynamics. Nature 443, 651–657.

Doubravska, L., Krausova, M., Gradl, D., Vojtechova, M., Tumova, L., Lukas, J., Valenta, T., Pospichalova, V., Fafilek, B., Plachy, J., Sebesta, O., Korinek, V., 2011. Fatty acid modification of Wnt1 and Wnt3a at serine is prerequisite for lipidation at cysteine and is essential for Wnt signalling. Cell. Signal. 23, 837–848.

Ellens, H., Bentz, J., Mason, D., Zhang, F., White, J.M., 1990a. Fusion of influenza hemagglutinin-expressing fibroblasts with glycophorin-bearing liposomes - role of hemagglutinin surface-density. Biochemistry 29, 9697–9707.

Ellens, H., Bentz, J., Mason, D., Zhang, F., White, J.M., 1990b. Fusion of influenza hemagglutinin-expressing fibroblasts with glycophorin-bearing liposomes: role of hemagglutinin surface density. Biochemistry 29, 9697–9707.

Floyd, D.L., Ragains, J.R., Skehel, J.J., Harrison, S.C., van Oijen, A.M., 2008. Single-particle kinetics of influenza virus membrane fusion. Proc. Natl. Acad. Sci. U.S.A. 105, 15382–15387.

Fu, Q., Xiang, Y.K., 2015. Chapter seven - trafficking of β-adrenergic receptors: implications in intracellular receptor signaling. In: Wu, G. (Ed.), Progress in Molecular Biology and Translational Science. Academic Press, pp. 151–188.

Fujioka, Y., Tsuda, M., Nanbo, A., Hattori, T., Sasaki, J., Sasaki, T., Miyazaki, T., Ohba, Y., 2013. A Ca(2+)-dependent signalling circuit regulates influenza A virus internalization and infection. Nat. Commun. 4, 2763.

Fujisaki, S., Takashita, E., Yokoyama, M., Taniwaki, T., Xu, H., Kishida, N., Sato, H., Tashiro, M., Imai, M., Odagiri, T., 2012. A single E105K mutation far from the active site of influenza B virus neuraminidase contributes to reduced susceptibility to multiple neuraminidase-inhibitor drugs. Biochem. Biophys. Res. Commun. 429, 51–56.

Furuishi, K., Matsuoka, H., Takama, M., Takahashi, I., Misumi, S., Shoji, S., 1997. Blockage of N-myristoylation of HIV-1 gag induces the production of impotent progeny virus. Biochem. Biophys. Res. Commun. 237, 504–511.

Gadalla, M.R., Abrami, L., van der Goot, F.G., Veit, M., 2020. Hemagglutinin of Influenza A, but not of Influenza B and C viruses is acylated by ZDHHC2, 8, 15 and 20. Biochem. J. 477, 285–303.

Gadalla, M.R., Veit, M., 2020. Toward the identification of ZDHHC enzymes required for palmitoylation of viral protein as potential drug targets. Expet Opin. Drug Discov. 15, 159–177.
Gambhir, A., Hangyas-Mihalyne, G., Zaitseva, I., Cafiso, D.S., Wang, J., Murray, D., Pentyala, S.N., Smith, S.O., McLaughlin, S., 2004. Electrostatic sequestration of PIP2 on phospholipid membranes by basic/aromatic regions of proteins. Biophys. J. 86, 2188–2207.
Gc, J.B., Gerstman, B.S., Stahelin, R.V., Chapagain, P.P., 2016. The Ebola virus protein VP40 hexamer enhances the clustering of PI(4,5)P-2 lipids in the plasma membrane. Phys. Chem. Chem. Phys. 18, 28409–28417.
Gudheti, M.V., Curthoys, N.M., Gould, T.J., Kim, D., Gunewardene, M.S., Gabor, K.A., Gosse, J.A., Kim, C.H., Zimmerberg, J., Hess, S.T., 2013. Actin mediates the nanoscale membrane organization of the clustered membrane protein influenza hemagglutinin. Biophys. J. 104, 2182–2192.
Gunewardene, M.S., Subach, F.V., Gould, T.J., Penoncello, G.P., Gudheti, M.V., Verkhusha, V.V., Hess, S.T., 2011. Superresolution imaging of multiple fluorescent proteins with highly overlapping emission spectra in living cells. Biophys. J. 101, 1522–1528.
Gurskaya, N.G., Verkhusha, V.V., Shcheglov, A.S., Staroverov, D.B., Chepurnykh, T.V., Fradkov, A.F., Lukyanov, S., Lukyanov, K.A., 2006. Engineering of a monomeric green-to-red photoactivatable fluorescent protein induced by blue light. Nat. Biotechnol. 24, 461–465.
Hale, B.G., Batty, I.H., Downes, C.P., Randall, R.E., 2008. Binding of influenza A virus NS1 protein to the inter-SH2 domain of p85 suggests a novel mechanism for phosphoinositide 3-kinase activation. J. Biol. Chem. 283, 1372–1380.
Hamilton, B.S., Whittaker, G.R., Daniel, S., 2012. Influenza virus-mediated membrane fusion: determinants of hemagglutinin fusogenic activity and experimental approaches for assessing virus fusion. Viruses 4, 1144–1168.
Heo, W.D., Inoue, T., Park, W.S., Kim, M.L., Park, B.O., Wandless, T.J., Meyer, T., 2006. PI(3,4,5)P-3 and PI(4,5)P-2 lipids target proteins with polybasic clusters to the plasma membrane. Science 314, 1458–1461.
Hess, S.T., Girirajan, T.P., Mason, M.D., 2006. Ultra-high resolution imaging by fluorescence photoactivation localization microscopy. Biophys. J. 91, 4258–4272.
Hoffmann, M., Kleine-Weber, H., Pohlmann, S., 2020a. A multibasic cleavage site in the spike protein of SARS-CoV-2 is essential for infection of human lung cells. Mol Cell 78, 779–784 e775.
Hoffmann, M., Kleine-Weber, H., Schroeder, S., Kruger, N., Herrler, T., Erichsen, S., Schiergens, T.S., Herrler, G., Wu, N.H., Nitsche, A., Muller, M.A., Drosten, C., Pohlmann, S., 2020b. SARS-CoV-2 cell entry depends on ACE2 and TMPRSS2 and is blocked by a clinically proven protease inhibitor. Cell 181, 271–280 e278.
Hu, S., He, X., Nie, J., Hou, J., Wu, J., Liu, X., Wei, Y., Tang, H., Sun, W., Zhou, S., Yuan, Y., An, Y., G, Y., Lin, Y., Lin, P., Zhao, J., Ye, M., Zhao, J., Xu, W., Zhao, S., 2022. Methylene-bridge tryptophan fatty acylation regulates PI3K-AKT signaling and glucose uptake. Cell Rep. 38.
Ito, H., Watanabe, S., Takada, A., Kawaoka, Y., 2001. Ebola virus glycoprotein: proteolytic processing, acylation, cell tropism, and detection of neutralizing antibodies. J. Virol. 75, 1576–1580.
Jin, H., Leser, G.P., Lamb, R.A., 1994. The influenza virus hemagglutinin cytoplasmic tail is not essential for virus assembly or infectivity. EMBO J. 13, 5504–5515.
Jin, H., Leser, G.P., Zhang, J., Lamb, R.A., 1997. Influenza virus hemagglutinin and neuraminidase cytoplasmic tails control particle shape. EMBO J. 16, 1236–1247.
Jin, H., Subbarao, K., Bagai, S., Leser, G.P., Murphy, B.R., Lamb, R.A., 1996. Palmitylation of the influenza virus hemagglutinin (H3) is not essential for virus assembly or infectivity. J. Virol. 70, 1406–1414.
Jo, S., L, J.B., Klauda, J.B., Im, W., 2009. CHARMM-GUI membrane builder for mixed bilayers and its application to yeast membranes. Biophys. J. 97, 50–58.
Jo, S., Kim, T., Im, W., 2007. Automated builder and database of protein/membrane complexes for molecular dynamics simulations. PLoS One 2 (9), e880.
Jo, S., Kim, T., Iyer, V.G., Im, W., 2008. CHARMM-GUI: a web-based graphical user interface for CHARMM. J. Comput. Chem. 29, 1859–1865.
Johnson, K.A., Taghon, G.J., Scott, J.L., Stahelin, R.V., 2016. The Ebola Virus matrix protein, VP40, requires phosphatidylinositol 4,5-bisphosphate (PI(4,5)P2) for extensive oligomerization at the plasma membrane and viral egress. Sci. Rep. 6, 19125.
Jumper, J., Evans, R., Pritzel, A., al, e., 2021. Highly accurate protein structure prediction with AlphaFold. Nature 596, 583–589.
Kang, Y.L., Chou, Y.Y., Rothlauf, P.W., Liu, Z., Soh, T.K., Cureton, D., Case, J.B., Chen, R. E., Diamond, M.S., Whelan, S.P.J., Kirchhausen, T., 2020. Inhibition of PIKfyve kinase prevents infection by Zaire ebolavirus and SARS-CoV-2. Proc. Natl. Acad. Sci. U.S.A. 117, 20803–20813.
Korber, B., Fischer, W., Gnanakaran, S., Yoon, H., Theiler, J., Abfalterer, W., Foley, B., Giorgi, E., Bhattacharya, T., Parker, M., Partridge, D., Evans, C., de Silva, T., 2020a. Spike Mutation Pipeline Reveals the Emergence of a More Transmissible Form of SARS-CoV-2. bioRxiv.
Korber, B., Fischer, W.M., Gnanakaran, S., Yoon, H., Theiler, J., Abfalterer, W., Hengartner, N., Giorgi, E.E., Bhattacharya, T., Foley, B., Hastie, K.M., Parker, M.D., Partridge, D.G., Evans, C.M., Freeman, T.M., de Silva, T.I., Sheffield, C.-G.G., McDanal, C., Perez, L.G., Tang, H., Moon-Walker, A., Whelan, S.P., LaBranche, C.C., Saphire, E.O., Montefiori, D.C., 2020b. Tracking changes in SARS-CoV-2 spike: evidence that D614G increases infectivity of the COVID-19 virus. Cell 182, 812–827 e819.
Krishnankutty, R.K., Kukday, S.S., Castleberry, A.J., Breevoort, S.R., Schmidt, W.K., 2009. Proteolytic processing of certain CaaX motifs can occur in the absence of the Rce1p and Ste24p CaaX proteases. Yeast 26, 451–463.
Lee, J., Patel, D.S., Ståhle, J., Park, S.-J., Kern, N.R., Kim, S., Lee, J., Cheng, X., Valvano, M.A., Holst, O., Knirel, Y., Qi, Y., Jo, S., Klauda, J.B., Widmalm, G., Im, W., 2019. CHARMM-GUI membrane builder for complex biological membrane simulations with glycolipids and lipoglycans. J. Chem. Theor. Comput. 15, 775–786.
Lee, J.E., Saphire, E.O., 2009. Ebolavirus glycoprotein structure and mechanism of entry. Future Virol. 4, 621–635.
Lemmon, M.A., 2008. Membrane recognition by phospholipid-binding domains. Nat. Rev. Mol. Cell Biol. 9, 99–111.
Levin, R., Hammond, G.R., Balla, T., De Camilli, P., Fairn, G.D., Grinstein, S., 2017. Multiphasic dynamics of phosphatidylinositol 4-phosphate during phagocytosis. Mol. Biol. Cell 28, 128–140.
Li, X., Shen, L., Xu, Z., Liu, W., Li, A., Xu, J., 2022. Protein palmitoylation modification during viral infection and detection methods of palmitoylated proteins. Front. Cell. Infect. Microbiol. 12, 821596.
Linder, M.E., Deschenes, R.J., 2007. Palmitoylation: policing protein stability and traffic. Nat. Rev. Mol. Cell Biol. 8, 74–84.
McBride, C.E., Machamer, C.E., 2010. Palmitoylation of SARS-CoV S protein is necessary for partitioning into detergent-resistant membranes and cell-cell fusion but not interaction with M protein. Virology 405, 139–148.
McCown, M.F., Pekosz, A., 2005. The influenza a Virus M-2 cytoplasmic tail is required for infectious virus production and efficient genome packaging. J. Virol. 79, 3595–3605.
McLaughlin, S., Murray, D., 2005. Plasma membrane phosphoinositide organization by protein electrostatics. Nature 438, 605–611.
McLaughlin, S., Wang, J., Gambhir, A., Murray, D., 2002. PIP(2) and proteins: interactions, organization, and information flow. Annu. Rev. Biophys. Biomol. Struct. 31, 151–175.
Melikyan, G.B., Jin, H., Lamb, R.A., Cohen, F.S., 1997. The role of the cytoplasmic tail region of influenza virus hemagglutinin in formation and growth of fusion pores. Virology 235, 118–128.
Naeve, C.W., Williams, D., 1990. Fatty acids on the A/Japan/305/57 influenza virus hemagglutinin have a role in membrane fusion. EMBO J. 9, 3857–3866.
Naim, H.Y., Amarneh, B., Ktistakis, N.T., Roth, M.G., 1992. Effects of altering palmitylation sites on biosynthesis and function of the influenza virus hemagglutinin. J. Virol. 66, 7585–7588.
National Library of Medicine (US), N.C.f.B.I, 1988. National center for biotechnology information (NCBI) Bethesda (MD). https://www.ncbi.nlm.nih.gov/.
Nayak, D.P., Hui, E.K.W., Barman, S., 2004. Assembly and budding of influenza virus. Virus Res. 106, 147–165.
Nobs, S.P., Schneider, C., Heer, A.K., Huotari, J., Helenius, A., Kopf, M., 2016. PI3Kgamma is critical for dendritic cell-mediated CD8+ T cell priming and viral clearance during influenza virus infection. PLoS Pathog. 12, e1005508.
O'Donnell, M.A., 2018. Tamas Balla: leading the way with phosphoinositides. J. Cell Biol. 217, 1161–1162.
O'Hanlon, R., Leyva-Grado, V.H., Sourisseau, M., Evans, M.J., Shaw, M.L., 2019. An influenza virus entry inhibitor targets class II PI3 kinase and synergizes with Oseltamivir. ACS Infect. Dis. 5, 1779–1793.
Obenauer, J.C., Denson, J., Mehta, P.K., Su, X.P., Mukatira, S., Finkelstein, D.B., Xu, X.Q., Wang, J.H., Ma, J., Fan, Y.P., Rakestraw, K.M., Webster, R.G., Hoffmann, E., Krauss, S., Zheng, J., Zhang, Z.W., Naeve, C.W., 2006. Large-scale sequence analysis of avian influenza isolates. Science 311, 1576–1580.
Ohno, Y., Kihara, A., Sano, T., Igarashi, Y., 2006. Intracellular localization and tissue-specific distribution of human and yeast DHHC cysteine-rich domain-containing proteins. Biochim. Biophys. Acta 1761, 474–483.
Ohuchi, M., Ohuchi, R., Sakai, T., Matsumoto, A., 2002. Tight binding of influenza virus hemagglutinin to its receptor interferes with fusion pore dilation. J. Virol. 76, 12405–12413.
Olety, B., Veatch, S.L., Ono, A., 2015. Phosphatidylinositol-(4,5)-Bisphosphate acyl chains differentiate membrane binding of HIV-1 gag from that of the phospholipase Cdelta1 pleckstrin homology domain. J. Virol. 89, 7861–7873.
Ono, A., Ablan, S.D., Lockett, S.J., Nagashima, K., Freed, E.O., 2004. Phosphatidylinositol (4,5) bisphosphate regulates HIV-1 Gag targeting to the plasma membrane. Proc. Natl. Acad. Sci. U. S. A. 101, 14889–14894.
Oprinca, G.C., Muja, L.A., 2020. Postmortem examination of three SARS-CoV-2-positive autopsies including histopathologic and immunohistochemical analysis. Int. J. Leg. Med.
Ou, X., Liu, Y., Lei, X., Li, P., Mi, D., Ren, L., Guo, L., Guo, R., Chen, T., Hu, J., Xiang, Z., Mu, Z., Chen, X., Chen, J., Hu, K., Jin, Q., Wang, J., Qian, Z., 2020. Characterization of spike glycoprotein of SARS-CoV-2 on virus entry and its immune cross-reactivity with SARS-CoV. Nat. Commun. 11, 1620.
Pabis, A., Rawle, R.J., Kasson, P.M., 2020. Influenza hemagglutinin drives viral entry via two sequential intramembrane mechanisms. Proc. Natl. Acad. Sci. U.S.A. 117, 7200–7207.
Pal, R., Reitz Jr., M.S., Tschachler, E., Gallo, R.C., Sarngadharan, M.G., Veronese, F.D., 1990. Myristoylation of gag proteins of HIV-1 plays an important role in virus assembly. AIDS Res. Hum. Retrovir. 6, 721–730.
Park, S., Choi, Y.K., Kim, S., Lee, J., Im, W., 2021. CHARMM-GUI membrane builder for lipid nanoparticles with ionizable cationic lipids and PEGylated lipids. J. Chem. Inf. Model. 61, 5192–5202.
Paules, C.I., Sullivan, S.G., Subbarao, K., Fauci, A.S., 2018. Chasing seasonal influenza - the need for a universal influenza vaccine. N. Engl. J. Med. 378, 7–9.
Piccardi, M., 2004. Background subtraction techniques: a review. In: IEEE International Conference on Systems, Man and Cybernetics, pp. 3099–3104.
Plante, J.A., Liu, Y., Liu, J., Xia, H., Johnson, B.A., Lokugamage, K.G., Zhang, X., Muruato, A.E., Zou, J., Fontes-Garfias, C.R., Mirchandani, D., Scharton, D., Bilello, J. P., Ku, Z., An, Z., Kalveram, B., Freiberg, A.N., Menachery, V.D., Xie, X., Plante, K.S., Weaver, S.C., Shi, P.Y., 2020. Spike mutation D614G alters SARS-CoV-2 fitness. Nature.

Port, F., Basler, K., 2010. Wnt trafficking: new insights into Wnt maturation, secretion and spreading. Traffic 11, 1265–1271.
Raut, P., Obeng, B., Waters, H., Zimmerberg, J., Gosse, J.A., Hess, S.T., 2022a. Phosphatidylinositol 4,5-bisphosphate mediates the Co-distribution of influenza A hemagglutinin and matrix protein M1 at the plasma membrane. Viruses 14.
Raut, P., Waters, H., Zimmberberg, J., Obeng, B., Gosse, J., Hess, S.T., 2022. Localization-based super-resolution microscopy reveals relationship between SARS-CoV2 spike and phosphatidylinositol (4,5)-bisphosphate. Proc. SPIE-Int. Soc. Opt. Eng. 11965, 1196503.
Raut, P., Weller, S.R., Obeng, B., Soos, B.L., West, B.E., Potts, C.M., Sangroula, S., Kinney, M.S., Burnell, J.E., King, B.L., Gosse, J.A., Hess, S.T., 2022b. Cetylpyridinium chloride (CPC) reduces zebrafish mortality from influenza infection: super-resolution microscopy reveals CPC interference with multiple protein interactions with phosphatidylinositol 4,5-bisphosphate in immune function. Toxicol. Appl. Pharmacol. 440, 115913.
Rozelle, A.L., Machesky, L.M., Yamamoto, M., Driessens, M.H.E., Insall, R.H., Roth, M.G., Luby-Phelps, K., Marriott, G., Hall, A., Yin, H.L., 2000. Phosphatidylinositol 4,5-bisphosphate induces actin-based movement of raft-enriched vesicles through WASP-Arp2/3. Curr. Biol. 10, 311–320.
Sakai, T., Ohuchi, R., Ohuchi, M., 2002. Fatty acids on the A/USSR/77 influenza virus hemagglutinin facilitate the transition from hemifusion to fusion pore formation. J. Virol. 76, 4603–4611.
Sharpe, H.J., Stevens, T.J., Munro, S., 2010. A comprehensive comparison of transmembrane domains reveals organelle-specific properties. Cell 142, 158–169.
Shemesh, R., Novik, A., Cohen, Y., 2010. Follow the leader: preference for specific amino acids directly following the initial methionine in proteins of different organisms. Dev. Reprod. Biol. 8, 180–189.
Shin, Y.-K., Liu, Q., Tikoo, S.K., Babiuk, L.A., Zhou, Y., 2007. Effect of the phosphatidylinositol 3-kinase/Akt pathway on influenza A virus propagation. J. Gen. Virol. 88, 942–950.
Stahelin, R.V., 2014. Membrane binding and bending in Ebola VP40 assembly and egress. Front. Microbiol. 5, 300.
Takada, R., Satomi, Y., Kurata, T., Ueno, N., Norioka, S., Kondoh, H., Takao, T., Takada, S., 2006. Monounsaturated fatty acid modification of Wnt protein: its role in Wnt secretion. Dev. Cell 11, 791–801.
Takeda, M., Leser, G.P., Russell, C.J., Lamb, R.A., 2003. Influenza virus hemagglutinin concentrates in lipid raft microdomains for efficient viral fusion. Proc. Natl. Acad. Sci. U.S.A. 100, 14610–14617.
Tang, T., Bidon, M., Jaimes, J.A., Whittaker, G.R., Daniel, S., 2020. Coronavirus membrane fusion mechanism offers a potential target for antiviral development. Antivir. Res. 178, 104792.
Tsoi, H., Li, L., Chen, Z.S., Lau, K.F., Tsui, S.K., Chan, H.Y., 2014. The SARS-coronavirus membrane protein induces apoptosis via interfering with PDK1-PKB/Akt signalling. Biochem. J. 464, 439–447.
Ujike, M., Huang, C., Shirato, K., Matsuyama, S., Makino, S., Taguchi, F., 2012. Two palmitylated cysteine residues of the severe acute respiratory syndrome coronavirus spike (S) protein are critical for S incorporation into virus-like particles, but not for M-S co-localization. J. Gen. Virol. 93, 823–828.
Veit, M., 2012. Palmitoylation of virus proteins. Biol. Cell. 104, 493–515.
Veit, M., Serebryakova, M.V., Kordyukova, L.V., 2013. Palmitoylation of influenza virus proteins. Biochem. Soc. Trans. 41, 50–55.
Wagner, R., Herwig, A., Azzouz, N., Klenk, H.D., 2005. Acylation-mediated membrane anchoring of avian influenza virus hemagglutinin is essential for fusion pore formation and virus infectivity. J. Virol. 79, 6449–6458.
Wainright, P.O., Perdue, M.L., Brugh, M., Beard, C.W., 1991. Amantadine resistance among hemagglutinin subtype 5 strains of avian influenza virus. Avian Dis. 35, 31–39.
Wang, X., Xu, W., Hu, G., Xia, S., Sun, Z., Liu, Z., Xie, Y., Zhang, R., Jiang, S., Lu, L., 2020. SARS-CoV-2 infects T lymphocytes through its spike protein-mediated membrane fusion. Cell. Mol. Immunol.
Woodley, K.T., Collins, M.O., 2021. Regulation and function of the palmitoyl-acyltransferase ZDHHC5. FEBS J. 288, 6623–6634.
Wu, E.L., Cheng, X., Jo, S., Rui, H., Song, K.C., Dávila-Contreras, E.M., Qi, Y., Lee, J., Monje-Galvan, V., Venable, R.M., Klauda, J.B., Im, W., 2014. CHARMM-GUI membrane builder toward realistic biological membrane simulations. J. Comput. Chem. 35, 1997–2004.
Wu, Q., Zhou, L., Sun, X., Yan, Z., Hu, C., Wu, J., Xu, L., Li, X., Liu, H., Yin, P., Li, K., Zhao, J., Li, Y., Wang, X., Li, Y., Zhang, Q., Xu, G., Chen, H., 2017. Altered lipid metabolism in recovered SARS patients twelve years after infection. Sci. Rep. 7, 9110.
Wu, Z., Z, Z., Wang, X., Zhang, J., Ren, C., Li, Y., Gao, L., Liang, X., Wang, P., Ma, C., 2021. Palmitoylation of SARS-CoV-2 S protein is essential for viral infectivity. Signal Transduct. Targeted Ther. 6, 231.
Xia, S., Liu, M., Wang, C., Xu, W., Lan, Q., Feng, S., Qi, F., Bao, L., Du, L., Liu, S., Qin, C., Sun, F., Shi, Z., Zhu, Y., Jiang, S., Lu, L., 2020. Inhibition of SARS-CoV-2 (previously 2019-nCoV) infection by a highly potent pan-coronavirus fusion inhibitor targeting its spike protein that harbors a high capacity to mediate membrane fusion. Cell Res. 30, 343–355.
Xu, Z., Shi, L., Wang, Y., Zhang, J., Huang, L., Zhang, C., Liu, S., Zhao, P., Liu, H., Zhu, L., Tai, Y., Bai, C., Gao, T., Song, J., Xia, P., Dong, J., Zhao, J., Wang, F.S., 2020. Pathological findings of COVID-19 associated with acute respiratory distress syndrome. Lancet Respir. Med. 8, 420–422.
Yang, Z.Y., Huang, Y., Ganesh, L., Leung, K., Kong, W.P., Schwartz, O., Subbarao, K., Nabel, G.J., 2004. pH-dependent entry of severe acute respiratory syndrome coronavirus is mediated by the spike glycoprotein and enhanced by dendritic cell transfer through DC-SIGN. J. Virol. 78, 5642–5650.
Yuen, C.K., Wong, W.M., Mak, L.F., Wang, X., Chu, H., Yuen, K.Y., Kok, K.H., 2020. Suppression of SARS-CoV-2 infection in ex-vivo human lung tissues by targeting class III phosphoinositide 3-kinase. J. Med. Virol. 93, 2076–2083.
Zhang, L., Jackson, C.B., Mou, H., Ojha, A., Peng, H., Quinlan, B.D., Rangarajan, E.S., Pan, A., Vanderheiden, A., Suthar, M.S., Li, W., Izard, T., Rader, C., Farzan, M., Choe, H., 2020. SARS-CoV-2 spike-protein D614G mutation increases virion spike density and infectivity. Nat. Commun. 11, 6013.
Zhu, L., Ly, H., Liang, Y., 2014. PLC-gamma1 signaling plays a subtype-specific role in postbinding cell entry of influenza A virus. J. Virol. 88, 417–424.
Zhu, L., Yuan, C., Ding, X., Xu, S., Yang, J., Liang, Y., Zhu, Q., 2016. PLC-gamma1 is involved in the inflammatory response induced by influenza A virus H1N1 infection. Virology 496, 131–137.
Zurcher, T., Luo, G., Palese, P., 1994. Mutations at palmitylation sites of the influenza virus hemagglutinin affect virus formation. J. Virol. 68, 5748–5754.